

# A Model Predictive Control for Path Tracking of Electronic-Four-Wheel Drive Vehicles

Giseo Park and Seibum B. Choi, *Member, IEEE*

**Abstract**—This paper proposes a path tracking controller to assist the electronic-four-wheel drive (e-4WD) vehicle in following the desired path profile. It utilizes only readily available in-vehicle sensors and a standalone global positioning system (GPS). Noteworthy, both the lateral distance error and the heading angle error between the desired path profile and the vehicle are calculated using only a standalone GPS. Therefore, the proposed algorithm can be easily applied to mass-produced e-4WD vehicles. A model predictive control (MPC) is selected as the controller type, which derives optimal control input considering both state and input constraints of in-wheel motor (IWM) in the e-4WD vehicle. Due to the advantage of this MPC predicting the vehicle's future dynamic behavior in advance, it is possible to output a more preemptive and stable yaw moment for vehicle path tracking. Finally, a weighted least square (WLS) allocation that is suitable for redundant actuator configuration is utilized to distribute the optimal IWM torques to the front left and right wheels of the e-4WD vehicle. The major contributions of the proposed control algorithm are as follows. 1) It is the first time in this paper that the MPC is applied to path tracking of e-4WD vehicles. 2) The condensed constraint matrix of the proposed MPC has a structure that can be easily applied to the linear programming. Using the CarSim simulation and the real-car based experiment, the effectiveness of the proposed MPC algorithm is verified by a comparative analysis. Thus, the high path tracking accuracy of the proposed algorithm is confirmed.

**Index Terms**— Electronic-four-wheel drive vehicle, in-wheel motor, model predictive control, weighted least square allocation, and path tracking.

## NOMENCLATURE

$\beta$	Vehicle sideslip angle.
$C_f$	Tire cornering stiffness of front axle.
$C_r$	Tire cornering stiffness of rear axle.
$p_e$	Vehicle position on east axis (NE global coordinates).
$p_n$	Vehicle position on north axis (NE global coordinates).
$r$	Vehicle yaw rate.
$s$	Vehicle distance along the path.
$GR_s$	Steering gear ratio.
$\delta_{SWA}$	Steering wheel angle.

$\delta_f$	Front steering angle.
$v_x$	Vehicle longitudinal velocity.
$\psi$	Vehicle heading angle.
$I_z$	Vehicle yaw moment of inertia.
$M_z$	Corrective yaw moment.
$R_e$	Tire effective rolling radius.
$t$	Track width.
$m$	Total mass of vehicle.
$l_f$	Distance between the CG and the front axle.
$l_r$	Distance between the CG and the rear axle.
$L$	Distance between the front and rear axles.
$T_m$	IWM torque.
$Q$	Weighting matrix in MPC.
$R$	Weighting matrix in MPC.
$N$	Number of prediction steps in MPC.
$e_y$	Lateral distance error between vehicle and desired path.
$e_\psi$	Heading error between vehicle and desired path.
$\mu_{max}$	Tire-road friction coefficient.
$a_x$	Vehicle longitudinal acceleration.
$a_y$	Vehicle lateral acceleration.
$g$	Gravitational acceleration.

## I. INTRODUCTION

CURRENTLY, vehicle chassis control technologies that ensure that the vehicle follows the desired path accurately have received great attention [1]. High path tracking accuracy allows the vehicle to safely escape the path quickly.

How accurately a vehicle follows a desired path profile is one of the major factors for evaluating the vehicle cornering agility [2]. Since most commercial vehicles are designed to exhibit an under-steering tendency for cornering [3], they often rotate with a radius larger than the desired path. In the corner section, the closer the distance between the vehicle and the desired position, the more agile the vehicle passes through the corner. Hence, when the driver's cornering operation causes insufficient vehicle lateral behavior (by entering inappropriate steering and longitudinal velocity commands), the path tracking controller can reduce the difference between the vehicle and the desired path profile, so that the vehicle can achieve ideal cornering, i.e., neutral-steering. Generally, the path tracking control tends to lead to more amount of yaw moment than normal yaw rate tracking control does in the same condition. This paper deals with improving path tracking accuracy for vehicle cornering agility, which we address with a precise mathematical model of vehicle lateral motion.

Manuscript received; revised; accepted. Date of publication; data of current version. This research was supported by the 2021 Research Fund of University of Ulsan; National Research Foundation of Korea (NRF) grant funded by the Korea government (MSIP) (No. 2017R1A2B4004116) and the BK21+ program through the NRF funded by the Ministry of Education of Korea.

Giseo Park is with the School of Mechanical Engineering, University of Ulsan, Ulsan 44610, Korea (e-mail: eloq123@ulsan.ac.kr). Seibum B. Choi (Corresponding Author) is with the Department of Mechanical Engineering, Korea Advanced Institute of Science and Technology, Daejeon 34141, Korea (e-mail: sbchoi@kaist.ac.kr).

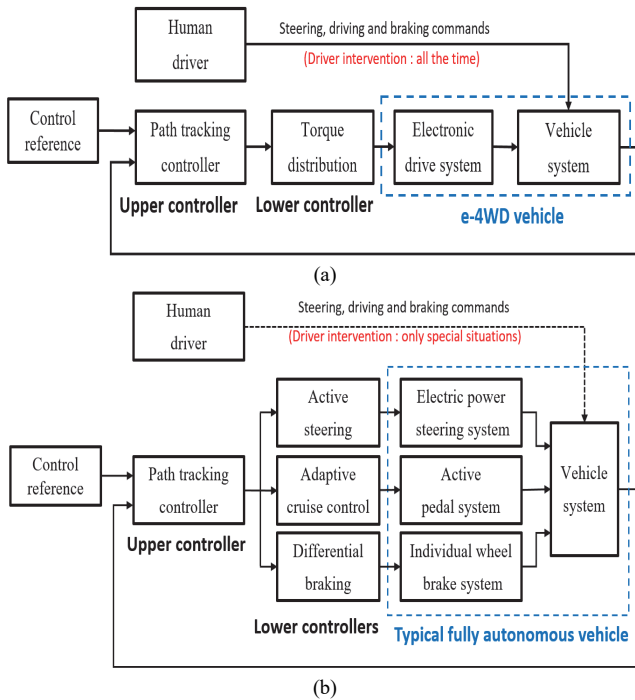


Fig. 1. Architecture diagrams: vehicle path tracking controllers of (a) e-4WD vehicle and (b) Typical fully autonomous vehicle.

The electronic-four-wheel drive (e-4WD) vehicle is a four-wheel drive vehicle with an electronic drive system [4]. A hybrid vehicle consisting of a mechanical drive system for two wheels and an electronic drive system for the other two is also classified as the e-4WD vehicle. The e-4WD vehicle varies the torque to each wheel independently, so that the difference between left and right hand side torques can assist the vehicle in following the desired path profile [5].

Figures 1 (a) and (b) show the architecture diagrams of vehicle path tracking controllers of e-4WD and typical fully autonomous vehicles, respectively. Unlike the path tracking of typical fully autonomous vehicles, which can be implemented without any driver intervention except in special situations, the path tracking of e-4WD vehicles has to be accompanied by the driver commands. As shown in Fig. 1 (a), generally, this system consists of an upper controller that generates the desired value of the corrective yaw moment and a lower controller that distributes it to each control actuator. In this paper, the path tracking control of such e-4WD vehicles is intensively dealt with.

#### A. System Configuration of e-4WD Vehicle

In-vehicle sensors and the standalone global positioning system (GPS) are utilized as sensors in the control system. Generally, commercial vehicles are equipped with some in-vehicle sensors, such as a steering wheel angle sensor, a gyroscope (yaw rate sensor), and wheel speed sensors; these are also the sensors required by the electronic stability control system (ESCs), which must be installed in the vehicle in accordance with vehicle regulations [6]. Also, both the lateral distance error and the heading angle error between the desired path profile and the vehicle are calculated in the control algorithm.

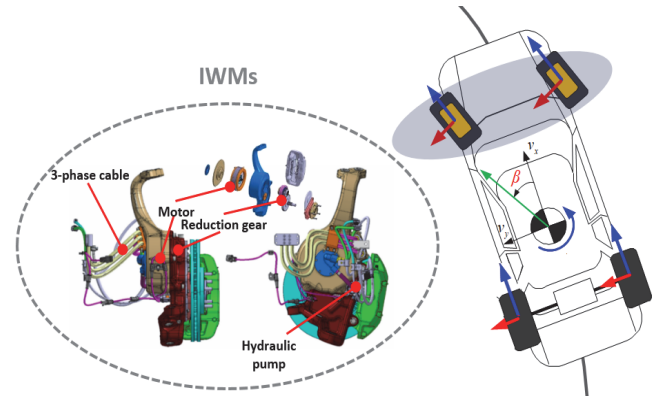


Fig. 2. IWMs in the front axle of e-4WD vehicle.

In this paper, the in-wheel motor system (IWMs) is used as the control actuator. As shown in Fig. 2, the e-4WD vehicle used in our study is equipped with IWMs on each front wheel. The rear wheels of this e-4WD vehicle are driven by mechanical driveline devices, such as an internal combustion engine, a torque converter, an automatic transmission, and an open differential. Acceleration and deceleration commands from a human driver generate equally distributed left and right rear wheel torques. Among the electronic drivetrains, the IWM has received great attention from many car makers over the last few decades, because of the following advantages [7]. 1) Both forward and reverse torques can be generated. This means that it is possible to drive and brake the vehicle. 2) The IWM can generate the wheel torque exactly as the driver requires. Such accurate wheel torque generation is an important factor in determining the accuracy of vehicle motion control. 3) Since there is no transmission device between the IWM and the vehicle wheel, the transfer efficiency of the IWM torque is very high [7-10]. This IWM has the potential to overcome the limitations of mechanical differential devices, such as slow response time and low torque transfer efficiency.

#### B. Literature Review

The following existing studies on vehicle path tracking select autonomous vehicles as targets. In [11] and [12], model predictive control (MPC) schemes using safe envelopes for obstacle avoidance and vehicle stability were proposed. Wang et al. [13] designed a composite nonlinear feedback strategy considering both tire force saturation and time-varying road curvatures; Guo et al. [14] dealt with an adaptive hierarchical control framework with an adaptive sliding mode control; and Hu et al. [15] proposed a robust H-infinity control strategy that is robust to the parametric uncertainties and external disturbances. In [16], a linear time varying-based MPC was presented with sideslip angle estimation by a sensor fusion for coordinated path tracking of autonomous electric vehicles. In addition, a MPC framework for collision avoidance in emergency situations and an integrated speed and steering controller for vehicle-driver closed-loop simulation were introduced in [17] and [18], respectively.

Existing studies dealing with path tracking of e-4WD vehicles are as follows. In [19], a direct yaw moment control based on driver behavior recognition was developed and its performance was experimentally verified on a lane change test. In addition,

an optimal control approach that minimized the objective function of tire force errors was introduced in [20], while [21] presented a robust H-infinity control approach with uncertainty analysis of vehicle modeling. However, these previous studies did not consider prediction of the future behavior of the vehicle, and thus was limited in terms of responsiveness of control input values. In [22], an optimal control algorithm that considered the effect of handling characteristics was designed for minimum time cornering. However, since it had a way of calculating the desired path with only vehicle model integration in real time, there was a risk that not using the reference position of desired path would generate an incorrect desired path when the vehicle model was inaccurate.

Considering these existing studies, it is concluded that an optimal control technique with the prediction of future vehicle behavior is necessary to achieve high control responsiveness for path tracking of e-4WD vehicles.

### C. Objectives

In line with the increasing demand for high cornering performance with price competitiveness, we aim to develop a path tracking controller of e-4WD vehicles, making both the lateral distance error and the heading angle error approach zero [21]. This is a practical vehicle control system that can be easily adapted to e-4WD vehicles with IWMs. Accordingly, the cornering agility of the e-4WD vehicle is expected to be improved by precisely tracking the pre-mapped path profile where drivers can drive at high speeds, such as on perimeter roads, highways and racing courses.

Since both the lateral distance error and the heading angle error between the desired path profile and the vehicle have to be controlled at the same time, the vehicle model is a multivariable system in which several vehicle state values are included as a state vector of the controller. Thus, an optimal controller is effective in minimizing a cost function in terms of control error of each state in a multi-variable control system.

Considering the real-car applicability, a linear MPC having no nonlinearity characteristics is selected as the controller type: it derives optimal control input while calculating future state values based on the vehicle model information.

### D. Contributions

The major contributions distinguishing the proposed control algorithm from the previous controllers are as follows.

1) Although the MPC has been already used in existing studies for path tracking of autonomous vehicles, it is the first time in this paper that the MPC is applied to path tracking of e-4WD vehicles. The MPC algorithm derives the optimal control input considering constraints of the e-4WD vehicle. Due to the characteristics of this MPC to predict the vehicle's future dynamic behavior in advance, it is possible to output a more preemptive and stable control input for vehicle path tracking. Finally, this point is verified by some real-car based experiments.

2) The condensed constraint matrix of the proposed MPC has a structure that can be easily applied to linear optimization

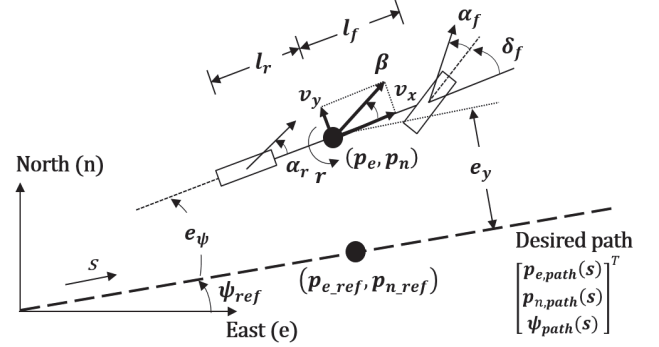


Fig. 3. Vehicle model schematic.

algorithms to perform the linear programming efficiently. Also, it considers both slew rate and amplitude constraints. This condensed constraint matrix of the linear MPC is used for the first time in this study for the purpose of vehicle path tracking. Also, the other minor one is that weighted least square (WLS) allocation, which minimizes the user-defined cost function with constraints of an IWM, is utilized for optimal torque distribution. It can also consider the control effort of the IWM.

This paper is comprised of six sections. Section II presents the overall system modeling. The proposed MPC algorithm for vehicle path tracking is introduced in Section III. In Section IV, algorithm verification is performed in the CarSim simulation. Then, Section V presents the experimental results. Finally, Section VI concludes the paper.

## II. SYSTEM MODELING

### A. Vehicle Model

In this section, we introduce the vehicle bicycle model, which combines the tire forces of both sides at the center line [23]. Generally, the bicycle model are derived as

$$\dot{\beta} = -\frac{c_f+c_r}{mv_x}\beta + \left(\frac{c_r l_r - c_f l_f}{mv_x^2} - 1\right)r + \frac{c_f}{mv_x}\delta_f \quad (1)$$

$$\dot{r} = \frac{c_r l_r - c_f l_f}{I_z}\beta - \frac{c_f l_f^2 + c_r l_r^2}{I_z v_x}r + \frac{c_f l_f}{I_z}\delta_f + \frac{M_z}{I_z}. \quad (2)$$

The vehicle model for path tracking is designed to extend this vehicle bicycle model. For this, the position states of the vehicle are defined in relation to the desired path, as shown in Fig. 3. Here  $[p_{e,path}(s) \ p_{n,path}(s) \ \psi_{path}(s)]^T$  is the desired path along the distance  $s$ : east and north coordinates  $p_{e,path}(s)$  and  $p_{n,path}(s)$  and heading angle  $\psi_{path}(s)$  of the desired path, respectively.

Also,  $e_y$  is the lateral distance error between the vehicle position  $(p_e, p_n)$  and the reference position  $(p_{e,ref}, p_{n,ref})$  and  $e_\psi$  is the heading angle error between vehicle heading angle  $\psi$  and reference heading angle  $\psi_{ref}$ :  $e_\psi = \psi - \psi_{ref}$ .

The equations in terms of both  $e_y$  and  $e_\psi$  are written as follows (assuming that  $e_\psi$  is small) [17]:

$$\dot{e}_y = v_x \sin(e_\psi) + v_y \cos(e_\psi) \approx v_x(e_\psi + \beta) \quad (3)$$

$$\dot{e}_\psi = r - \dot{\kappa}(s) \approx r - v_x \kappa(s) \quad (4)$$

where

$$\dot{s} = v_x \cos(e_\psi) - v_y \sin(e_\psi) \approx v_x. \quad (5)$$

Here, the curvature of the desired path at  $s$  is

$$\kappa(s) = \frac{d\psi_{ref}}{ds}. \quad (6)$$

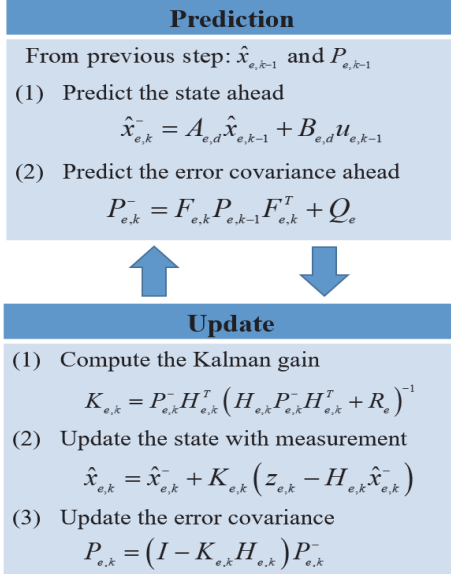


Fig. 4. Process of EKF.

Finally, by combining (1)-(5), a continuous state space representation of the vehicle model can be expressed as

$$\dot{x} = A_c x + B_c u + E_c \quad (7)$$

where

$$x = [\beta \quad r \quad e_y \quad e_\psi]^T, u = M_{z,des},$$

$$A_c = \begin{bmatrix} \frac{-(C_f+C_r)}{mv_x} & \frac{C_r l_r - C_f l_f}{mv_x^2} - 1 & 0 & 0 \\ \frac{C_r l_r - C_f l_f}{mv_x} & -(C_f l_f^2 + C_r l_r^2) & 0 & 0 \\ l_z & l_z v_x & 0 & v_x \\ 0 & 0 & 0 & 0 \end{bmatrix}, B_c = \begin{bmatrix} 0 \\ 1 \\ 0 \\ 0 \end{bmatrix}, \text{ and}$$

$$E_c = \begin{bmatrix} C_f \\ mv_x \\ C_f l_f \\ l_z \\ 0 \\ 0 \end{bmatrix} \delta_f + \begin{bmatrix} 0 \\ 0 \\ 0 \\ v_x \kappa(s) \end{bmatrix}.$$

Here,  $x \in \mathbb{R}^4$  and  $u \in \mathbb{R}$  are the state and control input vectors, respectively. Considering both the computational burden of MPC and the expansion of the number of IWMs in the future, the desired yaw moment  $M_{z,des}$ , not IWM torque, is determined as the control input. By the Euler method with the sampling time  $T_s$ , the state space representation (7) can be discretized at individual time step  $k$ :

$$x_{k+1} = A_d x_k + B_d u_k + E_d. \quad (8)$$

### B. Vehicle State Estimator

The vehicle state estimator to provide the estimated sideslip angle  $\hat{\beta}$  and heading angle  $\hat{\psi}$  is design based on the extended Kalman filter (EKF). The model equation with the state  $x_e$  and input  $u_e$  of the EKF is derived as follows [24].

$$\dot{x}_e = A_e x_e + B_e u_e \quad (9)$$

where

$$x_e = [\beta \quad r \quad \psi]^T, u_e = [\delta_f \quad M_z]^T,$$

$$A_e = \begin{bmatrix} \frac{-(C_f+C_r)}{mv_x} & \frac{C_r l_r - C_f l_f}{mv_x^2} - 1 & 0 \\ \frac{C_r l_r - C_f l_f}{mv_x} & -(C_f l_f^2 + C_r l_r^2) & 0 \\ l_z & l_z v_x & 0 \\ 0 & 1 & 0 \end{bmatrix}, \text{ and } B_e = \begin{bmatrix} C_f & 0 \\ mv_x & 1 \\ l_z & l_z \\ 0 & 0 \end{bmatrix}.$$

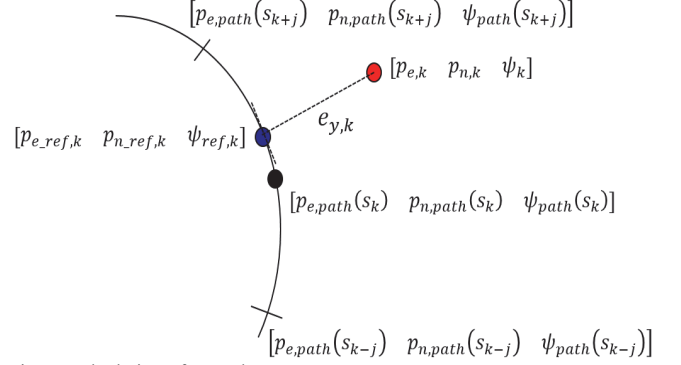


Fig. 5. Calculation of  $e_y$  and  $e_\psi$ .

With the sampling time  $T_s$ , (9) is discretized as:  $x_{e,k+1} = A_{e,d} x_{e,k} + B_{e,d} u_{e,k}$ . the measurement vector and output equation are given as below.

$$z_e = [r \quad a_y \quad v_e \quad v_n]^T \quad (10)$$

$$h_e(x_e, u_e) = \begin{bmatrix} r \\ \frac{-(C_f+C_r)}{m} \beta + \frac{C_r l_r - C_f l_f}{mv_x} r + \frac{C_f}{m} \delta_f \\ v_x (\cos(\psi) - \beta \sin(\psi)) \\ v_x (\sin(\psi) + \beta \cos(\psi)) \end{bmatrix} \quad (11)$$

As shown in Fig. 4, the discrete EKF consists of two steps, a prediction step and an update step. Here,  $Q_e$  and  $R_e$  are the covariance matrices of the process and measurement noises (assumed to be Gaussian white noises) and  $F_e$  and  $H_e$  are Jacobian matrices of model and output equations with respect to  $x_e$ , respectively. Lastly, the estimation targets  $\hat{\beta}$  and  $\hat{\psi}$  can be obtained from the EKF. Checking the observability of this nonlinear system [25], it is verified that the system is locally observable except when the vehicle is at rest or the vehicle drives straight.

### C. Calculation of Lateral Distance and Heading Angle Errors

In some previous papers [24, 26, 27], the precise vehicle positioning methods using in-vehicle sensors and standalone GPS were suggested to compensate for position error from the standalone GPS. Then, the vehicle position  $(p_e, p_n)$  estimated by the Kalman filter in [24] is utilized in this paper.

In order that  $e_y$  is accurately calculated, the reference vehicle position has to be accurately determined. We propose a method to determine the correct reference vehicle position  $(p_{e,ref,k}, p_{n,ref,k})$  at time step  $k$ . The vehicle distance after the  $k$  step from the start of driving is represented by  $s_k$ .

The distance from the vehicle position  $(p_{e,k}, p_{n,k})$  to the desired path  $(p_{e,path}(s_{k+i}), p_{n,path}(s_{k+i}))$  is as follows ( $i = -j, -j+1, \dots, 0, \dots, j-1, j$ ).

$$d_{k+i} = \sqrt{(p_{e,k} - p_{e,path}(s_{k+i}))^2 + (p_{n,k} - p_{n,path}(s_{k+i}))^2} \quad (12)$$

Among the candidates  $d_{k+i}$ , one has to be chosen as the minimum distance (see Fig. 5). The total number of candidates is  $2j+1$ . With an increasing  $j$ , a more accurate minimum distance can be found, but the amount of calculation increases.

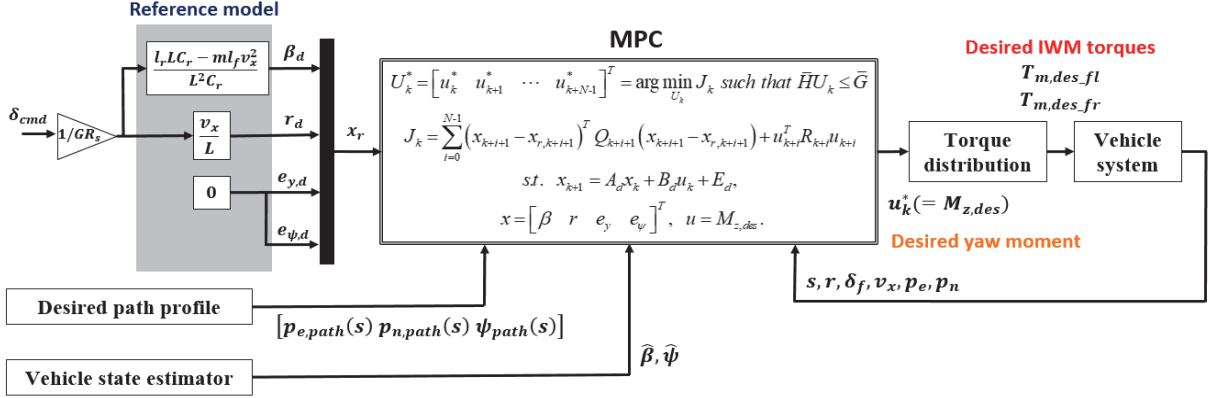


Fig. 6. Overall architecture of the proposed MPC algorithm.

Thus, the minimum distance  $d_{k+i^*}$  and the reference value  $[p_{e,ref,k} \ p_{n,ref,k} \ \psi_{ref,k}]$  at time step  $k$  are as follows:

$$d_{k+i^*} = \min(d_{k-j}, d_{k-j+1}, \dots, d_k, \dots, d_{k+j-1}, d_{k+j}) \quad (13)$$

$$[p_{e,ref,k} \ p_{n,ref,k} \ \psi_{ref,k}] = [p_{e,path}(s_{k+i^*}) \ p_{n,path}(s_{k+i^*}) \ \psi_{path}(s_{k+i^*})]. \quad (14)$$

Finally, both  $e_{y,k}$  and  $e_{\psi,k}$  at time step  $k$  can be obtained as follows.

$$e_{\psi,k} = \psi_k - \psi_{path}(s_{k+i^*}) \quad (15)$$

$$e_{y,k} = \text{sign} \left( (p_{n,k} - p_{n,path}(s_{k+i^*})) \cos(\psi_{path}(s_{k+i^*})) - (p_{e,k} - p_{e,path}(s_{k+i^*})) \sin(\psi_{path}(s_{k+i^*})) \right) \cdot d_{k+i^*} \quad (16)$$

### III. CONTROLLER DESIGN

Block diagrams of the overall control algorithm are illustrated in Fig. 6. Generally, the steady states of the vehicle bicycle model (i.e.,  $\dot{\beta} = 0$  in (1) and  $\dot{r} = 0$  and  $M_z = 0$  in (2)) are considered the control references of the vehicle lateral motion control [28]:

$$r_{ss,bic} = \frac{v_x}{L + K_v v_x^2} \delta_f \quad (17)$$

$$\beta_{ss,bic} = \frac{l_r \left( 1 - \frac{m l_f v_x^2}{L l_r C_r} \right)}{L(1 + K_v v_x^2)} \delta_f \quad (18)$$

where the under-steer gradient is

$$K_v = \frac{m(l_r C_r - l_f C_f)}{L C_f C_r}. \quad (19)$$

According to  $K_v$ , the steering characteristics in steady state cornering are classified ( $K_v > 0$ : under-steering ( $|\alpha_f| > |\alpha_r|$ ),  $K_v = 0$ : neutral-steering ( $|\alpha_f| = |\alpha_r|$ ), and  $K_v < 0$ : over-steering ( $|\alpha_f| < |\alpha_r|$ )) [29].

To achieve ideal steady state cornering, the references of the yaw rate and sideslip angle are set to the neutral-steering characteristics ( $K_v = 0$ ) [30]. Therefore, it is expected that the difference between absolute tire slip angles of the front and rear axles ( $|\alpha_f| - |\alpha_r|$ ) can certainly be reduced. Also, the ESCs, the backup safety system certainly preventing the vehicle getting into urgent driving situations already exists, so that drivers do not have to worry about the risk of using these aggressive control references.

#### A. MPC Design

To implement the MPC algorithm, both the estimated vehicle states and the desired path profile are received. Also, the reference model  $x_r \in \mathbb{R}^4$  is transmitted to this MPC algorithm.

$$x_r = [\beta_d \ r_d \ e_{y,d} \ e_{\psi,d}]^T = \begin{bmatrix} L l_r C_r - m l_f v_x^2 & v_x \delta_{cmd} \\ L^2 C_r & L \delta_{cmd} \\ 0 & 0 \end{bmatrix} \begin{bmatrix} \delta_{cmd} \\ \delta_{cmd} \end{bmatrix}. \quad (20)$$

Based on the discrete time linear system in (8), the state space representation of  $x_r$  without the control input is described as:

$$x_{r,k+1} = A_d x_{r,k} + E_d. \quad (21)$$

The equations of the vehicle model (8) and the reference model (21) are propagated to future steps up to the  $N$ th [31]. A sufficiently compromised value of  $N$  between control error and computational burden is selected with simulation-based performance analysis. At time step  $k$ , the predicted state sequence  $X_k \in \mathbb{R}^{4N}$  with the present state  $x_k$  and the input sequence  $U_k \in \mathbb{R}^N$  can be explicitly expressed as:

$$X_k = S^x x_k + S^u U_k + S^e \quad (22)$$

where

$$X_k = [x_{k+1} \ x_{k+2} \ \dots \ x_{k+N}]^T, \quad U_k = [u_k \ u_{k+1} \ \dots \ u_{k+N-1}]^T, \quad S^x = \begin{bmatrix} A_d \\ A_d^2 \\ \vdots \\ A_d^N \end{bmatrix}_{[4N \times 4]}, \quad S^e = \begin{bmatrix} E_d \\ A_d E_d + E_d \\ \vdots \\ A_d^{N-1} E_d + \dots + E_d \end{bmatrix}_{[4N \times 1]}, \quad \text{and} \quad S^u = \begin{bmatrix} B_d & 0 & \dots & 0 \\ A_d B_d & B_d & \dots & 0 \\ \vdots & \vdots & \ddots & \vdots \\ A_d^{N-1} B_d & A_d^{N-2} B_d & \dots & B_d \end{bmatrix}_{[4N \times N]}.$$

Instead of predicting a driver's future steering angle command, it is assumed that the steering angle  $\delta_f$  in the term  $E_d$  is constant with the value at time step  $k$  during the propagation for prediction time span. Then, the cost function of the MPC in quadratic form at time step  $k$  can be expressed as follows [32]:

$$J_k = \sum_{i=0}^{N-1} (x_{k+i+1} - x_{r,k+i+1})^T Q_{k+i+1} (x_{k+i+1} - x_{r,k+i+1}) + \dots + \dots u_{k+i}^T R_{k+i} u_{k+i} \quad (23)$$

where  $Q \in \mathbb{R}^{4 \times 4}$  and  $R \in \mathbb{R}$  are the non-negative weighting matrices for the predicted state sequence and the input sequence, respectively. This (23) can be written in a compact form:

$$J_k = X_k^T \bar{Q}_k X_k + U_k^T \bar{R}_k U_k - 2 X_{r,k}^T \bar{Q}_k X_k + X_{r,k}^T \bar{Q}_k X_{r,k}. \quad (24)$$

The lumped weighting matrices  $\bar{Q}_k \in \mathbb{R}^{4N \times 4N}$  and  $\bar{R}_k \in \mathbb{R}^{N \times N}$  and the predicted reference sequence  $X_{r,k} \in \mathbb{R}^{4N}$  are respectively expressed as follows.

$$\bar{Q}_k = \text{diag}(Q_{k+1}, Q_{k+2}, \dots, Q_{k+N}) \quad (25)$$

$$\bar{R}_k = \text{diag}(R_k, R_{k+1}, \dots, R_{k+N-1}) \quad (26)$$

$$X_{r,k} = [x_{r,k+1} \quad x_{r,k+2} \quad \dots \quad x_{r,k+N}]^T \quad (27)$$

Since the main purpose of this MPC is to have both  $e_y$  and  $e_\psi$  approach zero,  $Q_{33}$  and  $Q_{44}$  are set to be larger than  $Q_{11}$  and  $Q_{22}$  (in the diagonal weighting matrix  $Q = \text{diag}(Q_{11}, Q_{22}, Q_{33}, Q_{44})$ ). Additionally, the error tracking performance is given priority over reducing the energy consumption of the control input, so the magnitude of  $R$  is set to a value much smaller than that of  $Q$  [33, 34].

The cost function can be redefined as follows (the deleted terms do not affect the value of the final optimal solution):

$$J_k^* = U_k^T ((S^u)^T \bar{Q}_k S^u + \bar{R}_k) U_k + \dots \\ \dots (x_k^T (S^x)^T \bar{Q}_k S^u + (S^e)^T \bar{Q}_k S^u - 2X_{r,k}^T \bar{Q}_k S^u) U_k. \quad (28)$$

### B. State and Input Constraints

The constraints of predicted state sequence  $X_{min}, X_{max} \in \mathbb{R}^{4N}$  and input sequence  $U_{min}, U_{max} \in \mathbb{R}^N$  are given as:

$$X_{min} = [x_{min} \quad x_{min} \quad \dots \quad x_{min}]^T \quad (29)$$

$$X_{max} = [x_{max} \quad x_{max} \quad \dots \quad x_{max}]^T \quad (30)$$

$$U_{min} = [u_{min} \quad u_{min} \quad \dots \quad u_{min}]^T \quad (31)$$

$$U_{max} = [u_{max} \quad u_{max} \quad \dots \quad u_{max}]^T \quad (32)$$

where the limits of the state and control input are described, respectively, by:

$$x_{min} \leq x_k \leq x_{max} \\ u_{min} \leq u_k \leq u_{max}.$$

Lastly, the slew rate of the control input has the following constraint:

$$\Delta u_{min} \leq u_{k+1} - u_k \leq \Delta u_{max}. \quad (33)$$

Both maximum and minimum values of state variables are determined to avoid the vehicle instability situation. The input constraints  $u_{max}$  and  $u_{min}$  are the maximum and minimum of the desired yaw moments and the rate of change of the control input is constrained by  $\Delta u_{max}$  and  $\Delta u_{min}$ .

Considering the above constraint conditions, the constraint of the input sequence  $U_k$  can be expressed in the following compact form:

$$\bar{H}_k U_k \leq \bar{G}_k \quad (34)$$

where the condensed forms of constraint matrices  $\bar{H}_k \in \mathbb{R}^{(12N-2) \times N}$  and  $\bar{G}_k \in \mathbb{R}^{12N-2}$  are as follows, respectively:

$$\bar{H}_k = [H_{X,max} \quad H_{X,min} \quad H_{U,max} \quad H_{U,min} \quad H_{\Delta u,max} \quad H_{\Delta u,min}]^T \quad (35)$$

$$\bar{G}_k = [G_{X,max} \quad G_{X,min} \quad G_{U,max} \quad G_{U,min} \quad G_{\Delta u,max} \quad G_{\Delta u,min}]^T. \quad (36)$$

Each component of  $\bar{H}_k$  and  $\bar{G}_k$  is as follows.

$$H_{X,max} = S^u_{[4N \times N]}, H_{X,min} = -H_{X,max}, \\ H_{U,max} = I_{[N \times N]}, H_{U,min} = -H_{U,max}, \\ H_{\Delta u,max} = \begin{bmatrix} -1 & 1 & 0 & \dots & \dots & 0 \\ 0 & -1 & 1 & 0 & \dots & 0 \\ \vdots & 0 & \ddots & \ddots & \ddots & 0 \\ \vdots & \vdots & \ddots & \ddots & \ddots & \vdots \\ 0 & \dots & \dots & 0 & -1 & 1 \end{bmatrix}_{[(N-1) \times N]},$$

$$H_{\Delta u,min} = -H_{\Delta u,max}, \\ G_{X,max} = (X_{max} - S^x x_k - S^e)_{[4N \times 1]}, \\ G_{X,min} = -(X_{min} - S^x x_k - S^e)_{[4N \times 1]}, \\ G_{U,max} = U_{max [N \times 1]}, G_{U,min} = -U_{min [N \times 1]}, \\ G_{\Delta u,max} = \Delta u_{max [(N-1) \times 1]}, \text{ and } G_{\Delta u,min} = -\Delta u_{min [(N-1) \times 1]}.$$

The optimal input sequence  $U_k^* \in \mathbb{R}^N$  is determined by minimizing the cost function  $J_k^*$  (28) while satisfying the constraint condition over a prediction time horizon:

$$U_k^* = \arg \min_{U_k} J_k = \arg \min_{U_k} J_k^* \text{ such that } \bar{H}_k U_k \leq \bar{G}_k. \quad (37)$$

Only the first component  $u_k^* \in \mathbb{R}$  in  $U_k^*$  is derived from the desired yaw moment, i.e.,  $M_{z,des} = u_k^*$  [35].

A quadratic programming (QP) is the process of optimizing (minimizing or maximizing) a quadratic objective function subject to linear constraints [36]:  $\min_x \frac{1}{2} x^T H_{QP} x + f_{QP} x$  such that  $A_{QP} x \leq b_{QP}$ . Here,  $H_{QP} = 2((S^u)^T \bar{Q}_k S^u + \bar{R}_k) \in \mathbb{R}^{N \times N}$  and  $f_{QP} = (x_k^T (S^x)^T \bar{Q}_k S^u + (S^e)^T \bar{Q}_k S^u - 2X_{r,k}^T \bar{Q}_k S^u)^T \in \mathbb{R}^N$  from (28) and  $A_{QP} = \bar{H}_k$  and  $b_{QP} = \bar{G}_k$  from (37).

To solve this QP problem, the interior-point-convex algorithm is utilized, which has many advantages, such as low memory usage and the ability to solve large matrix problems quickly. Its specific principle and procedure are detailedly presented in [37].

Table III in Appendix summarizes the used control parameters. Here,  $T_s$  and  $T_p$  are the size of the time step to execute the controller and the time step for the prediction model, respectively. Since  $N$  is the number of prediction steps, the prediction time of MPC can be expressed as  $NT_p$ , which is much shorter than the approximate 1.6 seconds known as the average of driver's perception response time [38].

### C. Torque Distribution

The actual yaw moment caused by the actual front IWM torques  $T_{m,fl\&fr}$  is  $M_{z,act} (= t(T_{m,fr} - T_{m,fl}) / (2R_e))$ , to make it as close to  $M_{z,des}$  as possible, a method dealing with control allocation of overactuated systems is utilized to distribute  $T_{m,des}$  to each IWM in real time. For this purpose, WLS allocation that minimizes the user-defined cost function with constraints on control inputs is used in this study. The constraints of torque distribution are as follows:

$$T_{m,des,i} \sim [T_{m,min,i} \quad T_{m,max,i}] \quad (i = fl, fr).$$

Also, the following points are considered in the definition of the cost function  $J_{WLS}$ .

1) The desired and actual yaw moments are the same:

$$M_{z,des} = M_{z,act}.$$

2) To reduce the intervention in the change in vehicle longitudinal velocity, the sum of control inputs is zero:

$$T_{m,des,fl} + T_{m,des,fr} = 0.$$

3) To reduce the control effort, the desired control input vector  $u_{d,WLS}$  is set to  $[0 \quad 0]^T$ .

With the weighting factors  $W_u, W_v \in \mathbb{R}^{2 \times 2}$ , the actual control input vector  $u_{WLS,k}^* \in \mathbb{R}^2$  of the WLS allocation at time step  $k$  is derived as follows [39]:

$$J_{WLS,k} = (u_{WLS,k} - u_{d_{WLS,k}})^T W_u (u_{WLS,k} - u_{d_{WLS,k}}) + \dots \\ \dots (B_{WLS} u_{WLS,k} - v_{WLS,k})^T W_v (B_{WLS} u_{WLS,k} - v_{WLS,k}) \quad (38)$$

$$u_{WLS,k}^* = \arg \min_{u_{WLS,k}} J_{WLS,k} \text{ such that } \underline{u} \leq u_{WLS,k} \leq \bar{u} \quad (39)$$

where

$$u_{WLS,k} = \begin{bmatrix} T_{m,des,fl} \\ T_{m,des,fr} \end{bmatrix}, B_{WLS} = \begin{bmatrix} 1 & 1 \\ -\frac{1}{2R_e} & \frac{1}{2R_e} \end{bmatrix},$$

$$\underline{u} = [T_{m,min,fl} \quad T_{m,min,fr}]^T, \\ \bar{u} = [T_{m,max,fl} \quad T_{m,max,fr}]^T,$$

$$u_{d,WLS,k} = [0 \quad 0]^T, \text{ and } v_{WLS,k} = [0 \quad M_{z,des}]^T.$$

The interior-point-convex algorithm introduced earlier is utilized to solve (39). It is expected that the WLS allocation method can generate actual yaw moment accurately.

#### D. Design of Comparison Target

To focus on an effect of model prediction, the comparison target is selected as an infinite-horizon linear quadratic regulator (LQR) controller, which is an optimal control method that minimizes the quadratic cost function [40]. Unlike the MPC algorithm introduced earlier, this LQR controller does not consider state and input constraints in its optimization process and does not include any model predictive information. The design process of the LQR controller is as follows. The error dynamics, the difference between (8) and (21) can be described as the following discrete-time linear system:

$$(x_{k+1} - x_{r,k+1}) = A_d(x_k - x_{r,k}) + B_d u_k. \quad (40)$$

Here, the pair  $(A_d, B_d)$  is stabilizable. The cost function of the infinite-horizon LQR controller is defined as

$$J_{LQR} = \sum_{k=1}^{\infty} (x_{k+1} - x_{r,k+1})^T Q_{LQR} (x_{k+1} - x_{r,k+1}) + \dots \\ \dots u_k^T R_{LQR} u_k \quad (41)$$

where the positive symmetric definite  $Q_{LQR} \in \mathbb{R}^{4 \times 4}$  and  $R_{LQR} \in \mathbb{R}$  represent the weightings of the control error and input, respectively. The optimal control input  $u_{LQR,k} \in \mathbb{R}^2$  of the LQR controller that minimizes the cost function (41) is given as follows.

$$u_{LQR,k} = -F_{LQR}(x_k - x_{r,k}) \quad (42)$$

Accordingly, the desired yaw moment  $M_{z,des,LQR} (=u_{LQR,k})$  consists only of the feedback term of the control error  $x_k - x_{r,k}$ . The controller gain  $F_{LQR} \in \mathbb{R}^{1 \times 4}$  and the unique positive definite solution of the discrete-time algebraic Riccati equation  $P_{LQR} \in \mathbb{R}^{4 \times 4}$  are respectively as follows:

$$F_{LQR} = (R_{LQR} + B_d^T P_{LQR,k} B_d)^{-1} B_d^T P_{LQR,k} A_d \quad (43) \\ P_{LQR,k+1} = Q_{LQR} + A_d^T P_{LQR,k} A_d - \dots$$

$$\dots A_d^T P_{LQR,k} B_d (R_{LQR} + B_d^T P_{LQR,k} B_d)^{-1} B_d^T P_{LQR,k} A_d. \quad (44)$$

To solve (44), the dynamic Riccati equation of the finite horizon case iterates until it converges. This LQR controller is also accompanied by the same torque distribution algorithm as in Section IV-C. Through the comparative study with the LQR controller, it is possible to clearly confirm the advantages of the proposed MPC: for a fair comparison,  $Q = Q_{LQR} = \text{diag}(1, 1, 5, 5) \cdot 10^9$  and  $R = R_{LQR} = 1$  (refer to Table III).

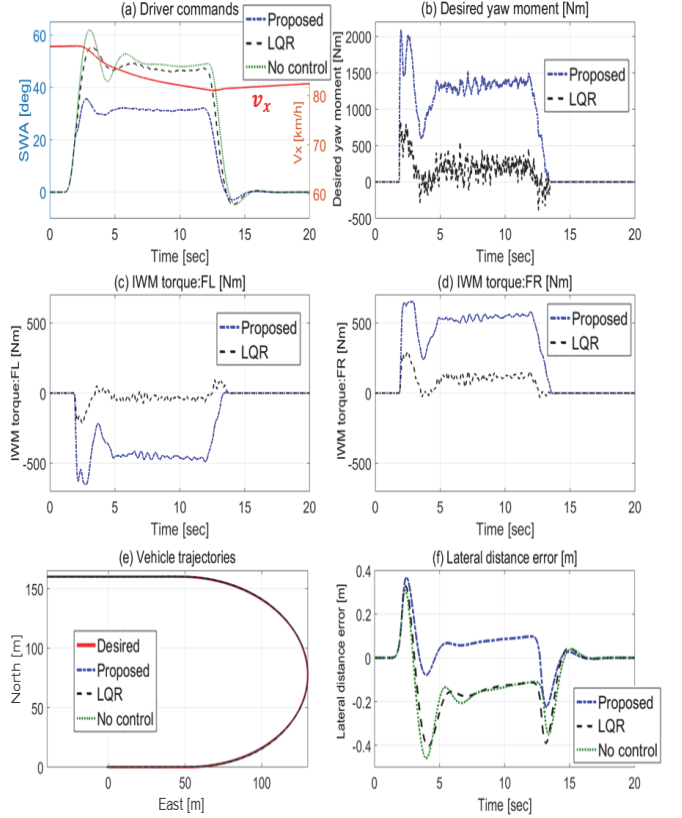


Fig. 7. Simulation results of circle turn test. (a) Driver commands. (b) Desired yaw moment. IWM torques: (c) FL and (d) FR. (e) Vehicle trajectories. (f) Lateral distance error.

#### IV. SIMULATION STUDY

Simulation studies are conducted to verify the superiority of the proposed MPC algorithm. CarSim (the vehicle dynamics software) and MATLAB/Simulink are utilized for the implementation of the simulation. The simulation vehicle is an E-class sedan with the parameters of an actual luxury sedan (refer to Table IV in Appendix). Its powertrain architecture is an e-4WD system consisting of IWMs in the front wheels and an engine driving the rear wheels. The tire model is the Magic Formula tire model [41].

The driving tests for the simulation verification are a circle turn, a double lane change (DLC), and closed-loop driving. Simulation studies on the circle turn and DLC are performed to evaluate the controller performance in the steady state cornering and transient state cornering, respectively.

The position information of each test course was stored on the control algorithm before the simulation implementation. The tire-road friction coefficient of the driving courses is given as  $\mu_{max} = 0.9$ . The steering commands from the CarSim driver model are set to the following values: a constant lateral distance offset of 0 m, a driver preview time of 1 s, a driver time lag of 0.11 s, a maximum steering wheel angle of 720 deg, and a maximum steering wheel angle rate of 1200 deg/s.

##### A. Circle Turn Test

The circle turn course consists of a circular road with a radius of 80 m and straight sections of entry and exit. As shown in Fig. 7 (a), the three control cases (the proposed MPC, LQR

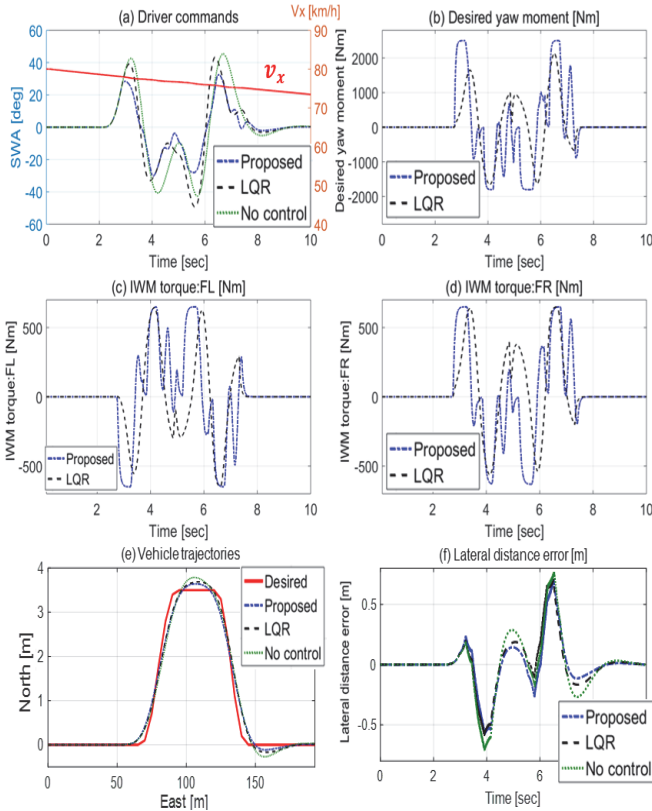


Fig. 8. Simulation results of DLC test. (a) Driver commands. (b) Desired yaw moment. IWM torques: (c) FL and (d) FR. (e) Vehicle trajectories. (f) Lateral distance error.

controller, and no control) have the same longitudinal velocity command, but the proposed algorithm leads to the smallest amount of steering commands. It is because that the large amount of  $M_{z,des}$  from the proposed MPC in Fig. 7 (b) greatly reduces the driver's steering effort.

In the case of the LQR controller, the extremely oscillatory  $M_{z,des\_LQR}$  is shown in Fig. 7 (b). This  $M_{z,des\_LQR}$  is a feedback error term with high-gain  $F_{LQR}$  (refer to (42)). Generally, the IWM has a low actuator bandwidth and motor backlash, so that the high-gain feedback applied to the IWMs often generates oscillatory control inputs especially in the steady state cornering when the control input quickly alternates between positive and negative. If  $F_{LQR}$  is further increased to increase the amount of  $M_{z,des\_LQR}$ , this oscillation issue is likely to become even more severe. Therefore, the LQR controller cannot generate as much IWM torque as the proposed MPC, as shown in Figs. 7 (c) and (d).

Although the difference between the vehicle trajectories is not apparent in Fig. 7 (e), the difference in the lateral distance errors in Fig. 7 (f) is clearly seen. In the initial section of the circular road where the transient state cornering occurs (i.e., the time interval of 4~6 s), the proposed MPC reflecting the future lateral behavior of the vehicle generates a greater amount of  $M_{z,des}$ , so that it leads to a much smaller lateral distance error. This also occurs in the time interval of 12~14 s at the end of the circular road. The results of the circle turn test shows that the proposed MPC algorithm has better control performance than the LQR controller in implementing accurate path tracking in steady state cornering.

## B. DLC Test

Figure 8 shows the path tracking results in the DLC test with severe transient steering maneuvers. As in the previous test, even in this DLC test, the proposed MPC requires the smallest amount of steering efforts (see Fig. 8 (a)).

Due to quickly changing steering commands, the proposed MPC generates the dynamically changing  $M_{z,des}$  in Fig. 8 (b) and preemptive IWM torques in Figs. 8 (c) and (d). On the other hand, in the case of the LQR controller, it can be seen that IWM torques that have a relatively slow response are output. It is evident in the initial cornering section when the DLC begins.

The final control results, the vehicle trajectory and the lateral distance error are shown in Figs. 8 (e) and (f), respectively. The vehicle trajectory from the proposed MPC is closest to the desired path profile, and this fact is clearly expressed at the reference points  $(p_{e\_ref}, p_{n\_ref}) = (110 \text{ m}, 3.5 \text{ m})$  and  $(160 \text{ m}, 0 \text{ m})$ .

For the uncontrolled case, the centrifugal force to the outside of the corner causes the vehicle to be pushed outwards from the desired path profile. In contrast, with the proposed MPC algorithm, the generated yaw moment prevents the vehicle from being pushed outward.

Differences in lateral distance errors are readily apparent at 4, 5, and 7.5 s in Fig. 8 (f). It can be confirmed that the proposed MPC has high path tracking performance in transient state cornering. As a result, the proposed MPC allows the vehicle to escape urgent DLC quickly and safely.

## C. Closed-Loop Driving Test

The last driving test is a relatively long-term driving test of about 120 s. The vehicle travels the flat racing course with evenly distributed straight and cornering sections. The driver model in simulation interface is set to have an aggressive driving tendency to actively exploit the friction circle of the tires (combining  $a_x$  and  $a_y$ ). The maximum values of vehicle longitudinal velocity and the master cylinder pressure are set to be 120 km/h and 10 MPa, respectively.

To clearly see how the vehicle trajectory is changed by the path tracking control, the simulation result of uncontrolled case is shown as a comparison target in Fig. 9.

In Fig. 9 (a), the proposed MPC leads to less steering effort of the driver. In addition, the vehicle speed profile of the proposed MPC is earlier than that of the uncontrolled case, so that it helps the vehicle complete a given closed-loop driving course faster, as shown in Fig. 9 (b). Figures 9 (e) and (f) show that the stable IWM torques are output without divergence or severe oscillation problems even during this high-speed driving.

Finally, as shown in Fig. 9 (h), the lateral distance error is noticeably reduced by the proposed MPC algorithm. Especially around 95 s, the proposed algorithm prevents the vehicle from being pushed out by the large centrifugal force. Figure 10 shows the differences between the vehicle trajectories in detail.

These results confirm that the proposed MPC algorithm greatly assists the vehicle in following the desired path profile correctly. Table I summarizes the simulation results in this Section V. It shows that the proposed MPC algorithm records the smallest root mean square (RMS) and maximum absolute

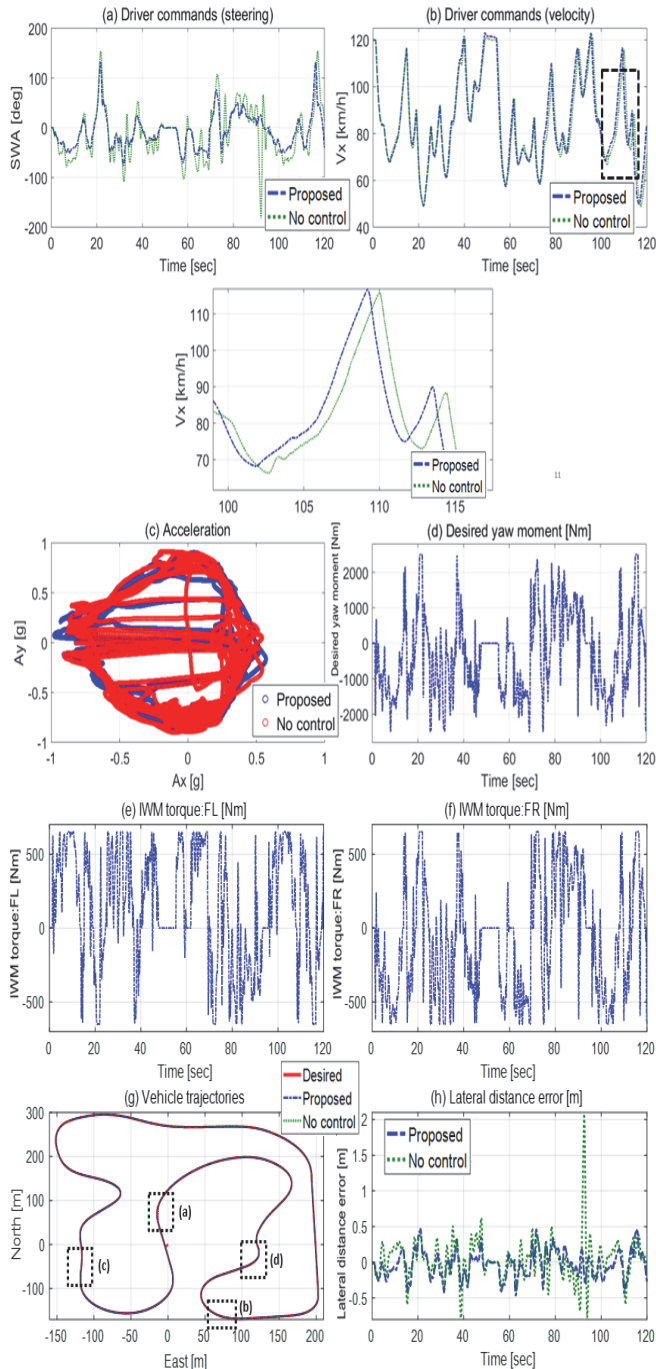


Fig. 9. Simulation results of closed-loop driving test. Driver commands: (a) Steering wheel angle and (b) Vehicle longitudinal velocity. (c) Accelerations. (d) Desired yaw moment. IWM torques: (e) FL and (f) FR. (g) Vehicle trajectories. (h) Lateral distance error.

TABLE I  
COMPARISON OF LATERAL DISTANCE ERROR (SIMULATION)

Test	Lateral distance error	Controller		
		No control	LQR	Proposed MPC
Circle turn	RMS [m]	0.168	0.159	0.097
	Max [m]	0.460	0.399	0.376
DLC	RMS [m]	0.205	0.194	0.188
	Max [m]	0.626	0.611	0.587
Closed-loop driving	RMS [m]	0.290	0.262	0.186
	Max [m]	2.079	1.936	0.470

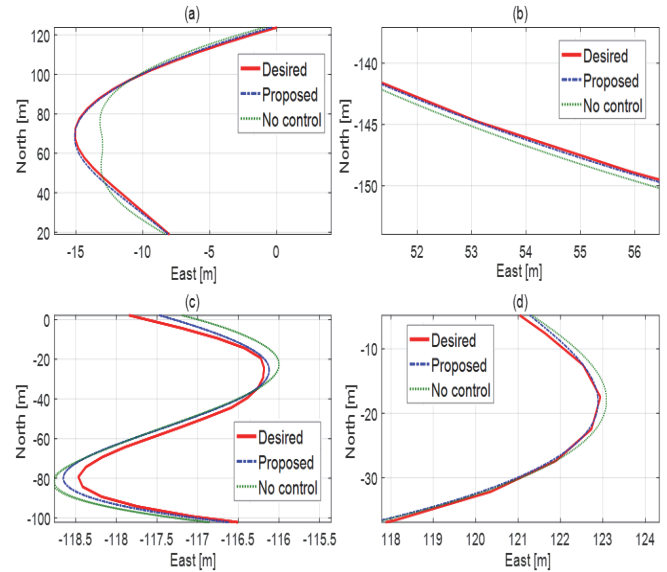


Fig. 10. Vehicle trajectories in closed-loop driving test.

values of the lateral distance error between the desired path profile and the vehicle.

As mentioned above, the LQR controller cannot generate as much yaw moment as the proposed MPC due to the oscillation issue in the steady state cornering so that its RMS and maximum errors in the closed-loop driving test are recorded as close to those of the uncontrolled case (it is not presented in Fig. 9 to highlight the control results of the proposed MPC).

## V. EXPERIMENTS

In this section, experiments are conducted to confirm whether the proposed algorithm is properly implemented in real vehicles. The Hyundai Genesis DH equipped with IWMs of the front wheels and the original rear wheel drive system was utilized as an experimental vehicle. As shown in Fig. 11 (a), the experimental vehicle consisting of IWM system, standalone GPS, Micro-AutoBox, and RT3002 (high precision differential GPS for algorithm verification) is set up. The sampling frequency of all used sensors is 100 Hz except that that of the standalone GPS is 10 Hz (it also increases up to 100 Hz with the filtering algorithm [24]). The proposed control algorithm in the Micro-AutoBox is as well implemented with a sampling frequency of 100 Hz on the controller area network (CAN).

The experimental vehicle drives on the high- $\mu_{max}$  closed-loop course in the Hyundai-Kia R&D center, which includes some steep curve sections (see Fig. 11 (b)). It usually takes about 85 seconds to complete one lap. The experimental vehicle starts driving at the coordinates  $(p_e, p_n) = (0 \text{ m}, 0 \text{ m})$  shown in Fig. 12 (e).

Figures 12 (a) and (b) shows the steering wheel angle and vehicle longitudinal velocity profiles, respectively. Similar to the simulation result in Fig. 9 (a), the proposed MPC algorithm only requires less steering effort than the uncontrolled case in Fig. 12 (a). Even in high-speed curve driving in the time interval of 10~15 s, since the proposed MPC predicts future vehicle behavior and driving path, it is possible to elicit a stable steering command.

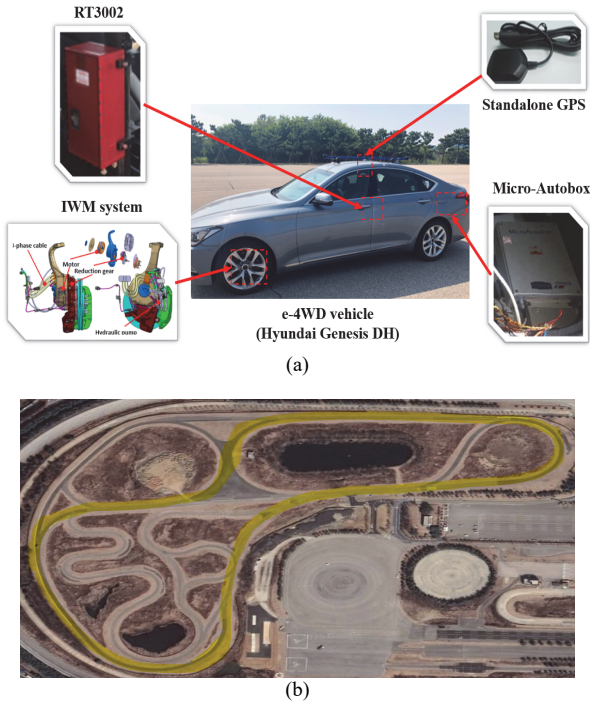


Fig. 11. Experimental environments (a) Set-up. (b) Closed-loop course.

TABLE II  
COMPARISON OF LATERAL DISTANCE ERROR (EXPERIMENT)

Test	Lateral distance error	Controller		
		No control	LQR	Proposed MPC
Closed-loop driving	RMS [m]	0.225	0.201	0.172
	Max [m]	1.212	1.165	1.015

Then, it is confirmed from Figs. 12 (c) and (d) that the IWM torque distribution is performed stably throughout the entire closed-loop driving. As shown in Fig. 12 (f), the RMS of the lateral distance error between the desired path profile and the vehicle is reduced with the proposed MPC algorithm. Figures 12 (g-j) show the main sections of Fig. 12 (e) on an enlarged scale. Table II including the experiment results of LQR controller summarizes the comparison of lateral distance error.

Through the experimental results of the closed-loop driving test, it is confirmed that the proposed MPC algorithm is developed appropriately enough to be implemented in real extreme driving situations.

## VI. CONCLUSION

The lateral motion controller for path tracking assists the vehicle in following the desired path profile. The proposed MPC algorithm derives the optimal control input considering both state and input constraints in the e-4WD vehicle. Also, a torque distribution method based on WLS allocation is designed, which derives optimal IWM torques considering the actuator limits of the IWMs.

Through simulation and experimental results with various driving scenarios on a high- $\mu_{max}$  surface, it is confirmed that the path tracking accuracy of the proposed MPC algorithm is improved over the other optimal control algorithm, the LQR controller.

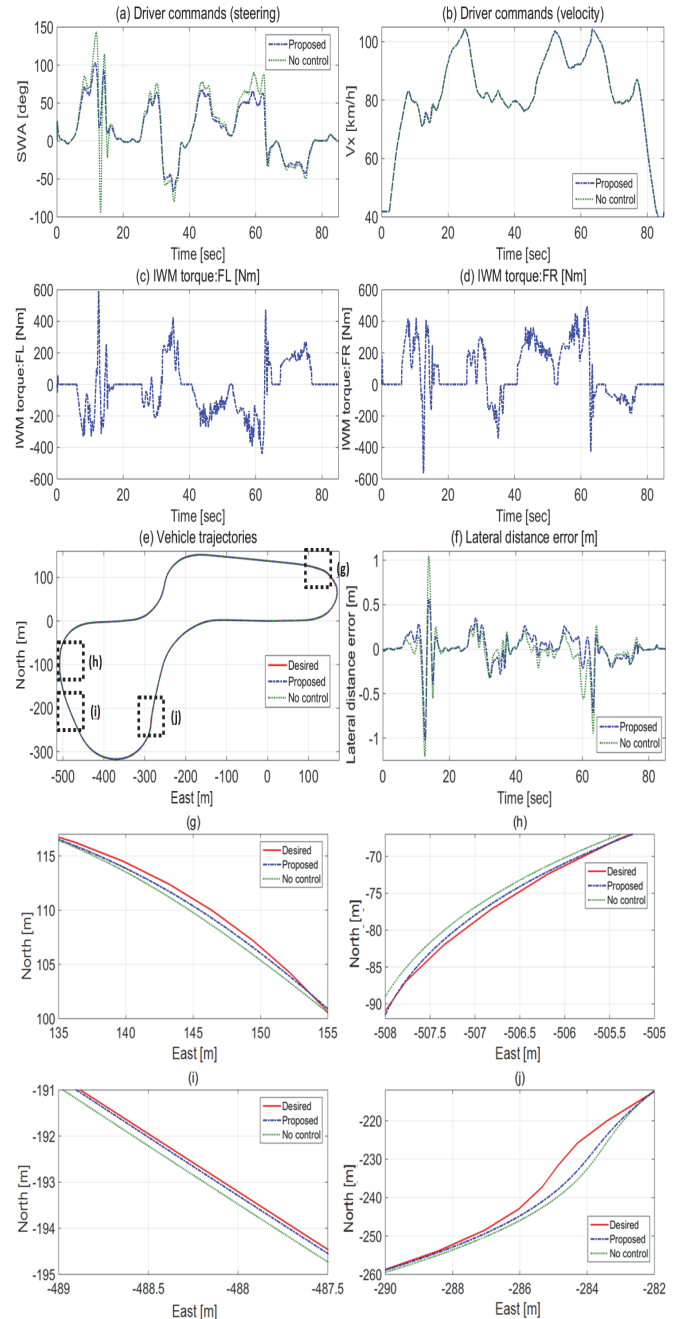


Fig. 12. Experimental results of closed-loop driving test. Driver commands: (a) Steering wheel angle and (b) Vehicle longitudinal velocity. IWM torques: (c) FL and (d) FR. (e) Vehicle trajectories. (f) Lateral distance error. Differences of vehicle trajectories: (g), (h), (i), and (j).

The major differences in the proposed path tracking algorithm distinguished from the existing algorithms are summarized as follows. 1) It utilizes only readily available in-vehicle sensors and standalone GPS, so it can be easily applied to mass-produced e-4WD vehicles. This point is advantageous for real-car application. 2) The proposed MPC algorithm predicts the vehicle lateral motion in advance, so that it is possible to output preemptive and accurate control action for high accuracy of vehicle path tracking. It is the first time in this paper that the MPC is applied to path tracking of e-4WD vehicles. Also, its condensed constraint matrix including both

slew rate and amplitude constraints has a structure that can be easily applied to the linear programming. 3) Since both MPC and WLS allocation are algorithms that minimize the cost functions, it is guaranteed that the optimal control action is finally output within various constraint conditions.

In conclusion, this paper demonstrates that the proposed path tracking algorithm can be a meaningful solution to enhance the cornering performance of e-4WD vehicles equipped with IWMs. Therefore, it is expected that even an ordinary driver can enjoy the fun-to-drive feeling and pass through corners as agilely as a skilled driver can.

#### APPENDIX

Control parameters and vehicle specifications used in simulation and experiment are presented in Tables III and IV, respectively.

TABLE III  
CONTROL PARAMETERS

Parameter	Value
$Q$	$diag(1, 1, 5, 5) \cdot 10^9$
$R$	1
$Q_{LQR}$	$diag(1, 1, 5, 5) \cdot 10^9$
$R_{LQR}$	1
$x_{max}$	$\left[ 10 \text{ deg } \frac{\mu_{max}g}{v_x} \text{ deg/s } 1.5 \text{ m } 20 \text{ deg} \right]^T$
$x_{min}$	$\left[ -10 \text{ deg } \frac{-\mu_{max}g}{v_x} \text{ deg/s } -1.5 \text{ m } -20 \text{ deg} \right]^T$
$u_{max}$	3000 Nm
$u_{min}$	-3000 Nm
$\Delta u_{max}$	10000 Nm/s
$\Delta u_{min}$	-10000 Nm/s
$N$	8
$T_s$	0.01 s
$T_p$	0.01 s
$W_u$	$diag(1, 1)$
$W_v$	$diag(10, 100)$
$T_{m,max,fl\&fr}$	650 Nm
$T_{m,min,fl\&fr}$	-650 Nm

TABLE IV  
VEHICLE SPECIFICATIONS

Parameter	Quantity	Value
$m$	Total vehicle mass	2280 kg
$l_f$	CG-front axle distance	1500 mm
$l_r$	CG-rear axle distance	1510 mm
$I_z$	Yaw moment of inertia	3234 kg · m <sup>2</sup>
$R_e$	Effective tire radius	353 mm
$t$	Track width	1600 mm
$C_f$	Tire cornering stiffness of front axle	155888 N/rad
$C_r$	Tire cornering stiffness of rear axle	156927 N/rad
$GR_s$	Steering gear ratio	21.1

#### REFERENCES

- [1] M. Ataei, A. Khajepour, and Soo Jeon, "A Novel Reconfigurable Integrated Vehicle Stability Control With Omni Actuation Systems," *IEEE Trans. Vehi. Technol.*, vol. 67, no. 4, pp. 2945-2957, 2018.
- [2] R. Pepy, A. Lambert, and H. Mounier, "Path Planning using a Dynamic Vehicle Model," in *Proc. International Conference on Information & Communication Technologies*, Damascus, Syria, 2006.
- [3] M. Jalali, E. Hashemi, A. Khajepour, S. Chen, and B. Litkouhi, "Integrated model predictive control and velocity estimation of electric vehicles," *Mechatronics*, vol. 46, pp. 84-100, 2017.
- [4] G. Park and S. B. Choi, "Development of a Torque Vectoring System in Hybrid 4WD Vehicles to Improve Vehicle Safety and Agility," in *Proc. Amer. Control Conf.*, Philadelphia, PA, USA, 2019.
- [5] L. Novellis, A. Sornioti, and P. Gruber, "Wheel Torque Distribution Criteria for Electric Vehicles With Torque-Vectoring Differentials," *IEEE Trans. Vehi. Technol.*, vol. 63, no. 4, pp. 1593-1602, 2014.
- [6] G. Park, S. Choi, D. Hyun, and J. Lee, "Integrated Observer Approach Using In-vehicle Sensors and GPS for Vehicle State Estimation," *Mechatronics*, vol. 50, pp. 134-147, 2018.
- [7] S. Murata, "Innovation by in-wheel-motor drive unit," *Vehi. Sys. Dyn.*, vol. 50, no. 6, pp. 807-830, 2012.
- [8] K. Nam, H. Fujimoto, and Y. Hori, "Lateral Stability Control of In-Wheel-Motor-Driven Electric Vehicles Based on Sideslip Angle Estimation Using Lateral Tire Force Sensors," *IEEE Trans. Vehi. Technol.*, vol. 61, no. 5, pp. 1972-1985, 2012.
- [9] B. Ren, H. Chen, H. Zhao, and L. Yuan, "MPC-based yaw stability control in in-wheel-motored EV via active front steering and motor torque distribution," *Mechatronics*, vol. 38, pp. 103-114, 2016.
- [10] K. Han, M. Choi, B. Lee, and S. Choi, "Development of a Traction Control System Using a Special Type of Sliding Mode Controller for Hybrid 4WD Vehicles," *IEEE Trans. Vehi. Technol.*, vol. 67, no. 1, pp. 264-274, 2018.
- [11] M. Brown, J. Funke, S. Erlien, and J. C. Gerdes, "Safe driving envelopes for path tracking in autonomous vehicles," *Control Engineering Practice*, vol. 61, pp. 307-316, 2017.
- [12] S. M. Erlien, S. Fujita, and J. C. Gerdes, "Shared Steering Control Using Safe Envelopes for Obstacle Avoidance and Vehicle Stability," *IEEE Trans. Intell. Transport. Syst.*, vol. 17, no. 2, pp. 441-451, 2016.
- [13] R. Wang, C. Hu, F. Yan, and M. Chadli, "Composite Nonlinear Feedback Control for Path Following of Four-Wheel Independently Actuated Autonomous Ground Vehicles," *IEEE Trans. Intell. Transport. Syst.*, vol. 17, no. 7, pp. 2063-2074, 2016.
- [14] J. Guo, Y. Luo, and K. Li, "An Adaptive Hierarchical Trajectory Following Control Approach of Autonomous Four-Wheel Independent Drive Electric Vehicles," *IEEE Trans. Intell. Transport. Syst.*, vol. 19, no. 8, pp. 2482-2492, 2018.
- [15] C. Hu, H. Jing, R. Wang, F. Yan, and M. Chadli, "Robust  $H_\infty$  output-feedback control for path following of autonomous ground vehicles," *Mech. Sys. and Sig. Process.*, vol. 70-71, pp. 414-427, 2016.
- [16] J. Guo, Y. Luo, K. Li, and Y. Dai, "Coordinated path-following and direct yaw-moment control of autonomous electric vehicles with sideslip angle estimation," *Mech. Sys. and Sig. Process.*, vol. 105, pp. 183-199, 2018.
- [17] J. Funke, M. Brown, S. M. Erlien, and J. C. Gerdes, "Collision Avoidance and Stabilization for Autonomous Vehicles in Emergency Scenarios," *IEEE Trans. Control Syst. Technol.*, vol. 25, no. 4, pp. 1204-1216, 2017.
- [18] Y. Koh, H. Her, K. Yi, and K. Kim, "Integrated Speed and Steering Control Driver Model for Vehicle-Driver Closed-Loop Simulation," *IEEE Trans. Vehi. Technol.*, vol. 65, no. 6, pp. 4401-4411, 2016.
- [19] P. Raksincharoensak, T. Mizushima, and M. Nagai, "Direct yaw moment control system based on driver behavior recognition," *Vehi. Sys. Dyn.*, vol. 46, pp. 911-921, 2008.
- [20] M. S. Fallah, A. Khajepour, B. Fidan, S. Chen, and B. Litkouhi, "Controller Development Using Optimal Torque Distribution for Driver Handling Assistance," in *Proc. Amer. Control Conf.*, Montreal, QC, Canada, 2012.
- [21] S. Khosravani, A. Kasaiezadeh, A. Khajepour, B. Fidan, S. Chen, and B. Litkouhi, "Torque-Vectoring-Based Vehicle Control Robust to Driver Uncertainties," *IEEE Trans. Vehi. Technol.*, vol. 64, no. 8, pp. 3359-3367, 2015.
- [22] E. N. Smith, E. Velenis, D. Tavernini, and D. Cao, "Effect of handling characteristics on minimum time cornering with torque vectoring," *Vehi. Sys. Dyn.*, vol. 56, no. 2, pp. 221-248, 2018.
- [23] Z. Wu, M. Yao, H. Ma, and W. Jia, "Improving Accuracy of the Vehicle Attitude Estimation for Low-Cost INS/GPS Integration Aided by the

- GPS-Measured Course Angle," *IEEE Trans. Intell. Transport. Syst.*, vol. 14, no. 2, pp. 553-564, 2013.
- [24] G. Park, Y. Hwang, and S. Choi, "Vehicle positioning based on velocity and heading angle observer using low-cost sensor fusion," *ASME J. Dyn. Syst., Meas., Control*, vol. 139, no. 12, pp. 1-13, 2017.
- [25] R. Hermann and A. Krener, "Nonlinear Controllability and Observability," *IEEE Trans. Auto. Con.*, vol. 22, no. 5, pp. 728-740, 1977.
- [26] K. Jo, K. Chu, and M. Sunwoo, "Interacting Multiple Model Filter-Based Sensor Fusion of GPS With In-Vehicle Sensors for Real-Time Vehicle Positioning," *IEEE Trans. Intell. Transport. Syst.*, vol. 13, no. 1, pp. 329-343, 2012.
- [27] K. Jo, M. Lee, and M. Sunwoo, "Road Slope Aided Vehicle Position Estimation System Based on Sensor Fusion of GPS and Automotive Onboard Sensors," *IEEE Trans. Intell. Transport. Syst.*, vol. 17, no. 1, pp. 250-263, 2016.
- [28] D. Piyabongkarn, R. Rajamani, J. Grogg, and J. Lew, "Development and Experimental Evaluation of a Slip Angle Estimator for Vehicle Stability Control," *IEEE Trans. Control Syst. Technol.*, vol. 17, no. 1, pp. 78-88, 2009.
- [29] R. Rajamani, *Vehicle Dynamics and control*. New York: Springer, 2006.
- [30] H. Her, Y. Koh, E. Joa, K. Yi, and K. Kim, "An Integrated Control of Differential Braking, Front/Rear Traction, and Active Roll Moment for Limit Handling Performance," *IEEE Trans. Vehi. Technol.*, vol. 65, no. 6, pp. 4288-4300, 2016.
- [31] M. Choi and S. B. Choi, "Mpc for vehicle lateral stability via differential braking and active front steering considering practical aspects," *IMEchE Part D: J Automobile Engineering*, vol. 230, no. 4, pp. 459-469, 2016.
- [32] F. Borrelli, A. Bemporad, and M. Morari, *Predictive control for linear and hybrid systems*. Cambridge University Press, 2017.
- [33] J. Kong, M. Pfeiffer, G. Schildbach, and F. Borrelli, "Kinematic and Dynamic Vehicle Models for Autonomous Driving Control Design," in *Proc. IEEE Intelligent Vehicles Symposium*, Seoul, Korea, 2016.
- [34] C. E. Beal and J. C. Gerdes, "Model predictive control for vehicle stabilization at the limits of handling," *IEEE Trans. Control Syst. Technol.*, vol. 21, no. 4, pp. 1258-1269, 2013.
- [35] F. Borrelli, A. Bemporad, M. Fodor, and D. Hrovat, "An mpc/hybrid system approach to traction control," *IEEE Trans. Control Syst. Technol.*, vol. 14, no. 3, pp. 541-552, 2006.
- [36] H. J. Ferreau, C. Kirches, A. Potschka, H. G. Bock, and M. Diehl, "qpOASES: a parametric active-set algorithm for quadratic programming," *Mathematical Programming Computation*, vol. 6, no. 4, pp. 327-363, 2014.
- [37] J. Lofberg, "Yalmip : a toolbox for modeling and optimization in matlab," in *Proc. IEEE International Conference on Robotics and Automation*, pp. 284-289, 2004.
- [38] P. L. Olson and M. Sivak, "Perception-Response Time to Unexpected Roadway Hazards," *Human Factors: The Journal of the Human Factors and Ergonomics Society*, vol. 28, no. 1, pp. 91-96, 1986.
- [39] G. Park and S. Choi, "Optimal Brake Distribution for Electronic Stability Control Using Weighted Least Square Allocation Method," in *Proc. Int. Conf. Con. Auto. Sys.*, Gyeongju, Korea, 2016.
- [40] A. Bemporad, M. Morari, V. Dua, and E. N. Pistikopoulos, "The explicit linear quadratic regulator for constrained systems," *Automatica*, vol. 38, no. 1, pp. 3-20, 2002.
- [41] G. Park, K. Han, K. Nam, H. Kim, and S. B. Choi, "Torque Vectoring Algorithm of Electronic-Four-Wheel Drive Vehicles for Enhancement of Cornering Performance," *IEEE Trans. Vehi. Technol.*, vol. 69, no. 4, pp. 3668-3679, 2020.



**Giseo Park** received the B.S. degree in mechanical engineering from Hanyang University, Seoul, Korea, in 2014 and the M.S. and Ph.D. degrees in mechanical engineering from Korea Advanced Institute of Science and Technology (KAIST), in 2016 and 2020. He was a senior engineer with Hyundai Motor Company, Hwasung, South Korea. He has been an assistant professor in the school of mechanical engineering from University of Ulsan, Ulsan, Korea. His research interests include vehicle dynamics, control theory, active safety systems and autonomous driving system.



**Seibum B. Choi** (M'09) received the B.S. degree in mechanical engineering from Seoul National University, Seoul, Korea; the M.S. degree in mechanical engineering from Korea Advanced Institute of Science and Technology (KAIST), Daejeon, Korea; and the Ph.D. degree in controls from the University of California, Berkeley, CA, USA, in 1993. Since 2006, he has been with the faculty of the Department of Mechanical Engineering, KAIST. His research interests include fuel-saving technology, vehicle dynamics and control, and active safety systems.